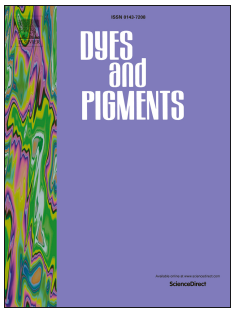

A porous tetraphenylethylene-based polymer for fast-response fluorescence sensing of Fe(III) ion and nitrobenzene

Yingting Zheng, Hailong Wang, Jianzhuang Jiang

PII: S0143-7208(19)31554-2

DOI: https://doi.org/10.1016/j.dyepig.2019.107929

Reference: DYPI 107929

To appear in: *Dyes and Pigments*

Received Date: 5 July 2019

Revised Date: 2 September 2019

Accepted Date: 23 September 2019

Please cite this article as: Zheng Y, Wang H, Jiang J, A porous tetraphenylethylene-based polymer for fast-response fluorescence sensing of Fe(III) ion and nitrobenzene, *Dyes and Pigments* (2019), doi: https://doi.org/10.1016/j.dyepig.2019.107929.

Graphical abstract

A porous tetraphenylethylene-based polymer for fast-response fluorescence sensing of Fe(III) ion and nitrobenzene

Yingting Zheng,[a] Hailong Wang,[a,*] and Jianzhuang Jiang[a,*]

A fluorescent porous tetraphenylethylene-based organic polymer (**PTOP**) was constructed and capable of exhibiting a fast-response and sensitive fluorescence sensing both Fe(III) and nitrobenzene.

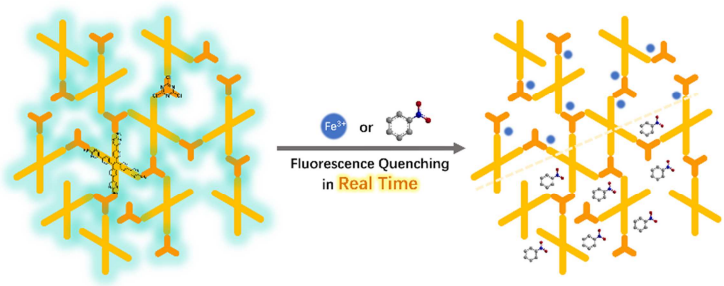

A porous tetraphenylethylene-based polymer for fast-response fluorescence sensing of Fe(III) ion and nitrobenzene

Yingting Zheng,[a] Hailong Wang,[a,*] and Jianzhuang Jiang[a,*]

[a] Beijing Key Laboratory for Science and Application of Functional Molecular and Crystalline Materials, Department of Chemistry, University of Science and Technology Beijing, Beijing 100083, China

[*] Corresponding author. E-mail: hlwang@ustb.edu.cn (H. Wang) and jianzhuang@ustb.edu.cn (J. Jiang)

Abstract: A fluorescent porous tetraphenylethylene-based organic polymer (**PTOP**) was constructed by the reaction of 5,5',5",5'"-(ethene-1,1,2,2-tetrayltetrakis(benzene-4,1-diyl))tetrakis(pyrimidin-2-amine) and cyanuric chloride in the presence of potassium carbonate. CO_2 sorption experiment at 195 K reveals the permanent porosity of **PTOP** with a Brunauer-Emmett-Teller surface area of 227 m^2 g^{-1}. In particular, the existence of rich secondary amines and pyrimidine nitrogen atoms surrounding the 1,3,5-triazine moieties in **PTOP** provides abundant chelating sites for metal ions, endowing a fast-response and sensitive fluorescence sensing Fe(III) with a low limit of detection of 4.5 μM. In addition, this polymer also shows an excellent sensing performance towards nitrobenzene with good selectivity and a low detection limit of 1.6 nM.

Keywords: tetraphenylethylene-based polymer; porous materials; fast-response Fe(III) sensing; nitrobenzene sensor

1. Introduction

Porous organic polymers (POPs), including a wide range of subspecies like hyper cross-linked polymers (HCPs),[1] polymers of intrinsic microporosity (PIMs),[2] covalent organic frameworks (COFs),[3]covalent triazine frameworks (CTFs),[4] conjugated microporous polymers (CMPs),[5,6] and porous aromatic frameworks (PAFs),[7–9] have been attracting increasing interests due to their great potential applications in gas adsorption and separation,[10–12] pollutes removal,[13] photoelectric conversion,[14] lithium battery,[15] sensing,[16] and catalysis.[17,18] On the other hand, aggregation-induced emission (AIE) molecular materials with potential applications in chemical sensing, bioprobes, and organic light-emitting diodes have also been intensively studied since the first discovery of AIE phenomenon by Tang and co-workers.[19–21] For the purpose of developing new fluorescence materials with enhanced emission and multifunctional properties, AIE luminogens (AIEgens) have been introduced/confined into various porous crystalline materials including hydrogen□bonded organic frameworks (HOFs),[22,23] COFs,[24] and metal organic frameworks (MOFs),[25,26] depending on hydrogen, covalent, and coordination bond interactions, respectively. As one of the representative AIEgens, tetraphenylethylene (TPE)[27,28] has also been introduced into the porous organic polymers[29] with excellent sensing performance. Despite the relatively extensive studies in this direction, developing new AIE-integrated POPs towards realizing their practical applications seems to be an important and ever-lasting duty for chemists and material scientists.

It is well-known that iron ion plays an important role in human life activities including various metabolic processes, brain and muscle functions, and transcription and translation of DNA and RNA.[30,31] However, excessively taking Fe^{3+} would cause serious health issues including insomnia, skin diseases, and immunity descent.[32] In addition, nitroaromatic

compounds (NACs) have been broadly employed in dye, firework, pharmaceutical and leather industry.[32,33] The relevant pollution emissions severely contaminate the water and soils and thus seriously threaten the human beings health.[33] As a consequence, great efforts have been paid in the exploration of new fluorescence sensors for both species, resulting in various kinds of Fe^{3+} and NACs fluorescence sensing materials in the past years.[31–34] Although some reports cover the AIE-confined fluorescence POPs for sensing small molecules and heavy metals,[35,36] very few investigations are about the detection of Fe^{3+} and NACs. As a result, more efforts are still necessary in this regard for the real applications.

Herein, by means of a newly developed TPE building block, 5,5',5",5"'-(ethene-1,1,2,2-tetrayltetrakis(benzene-4,1-diyl))tetrakis(pyrimidin-2-amine) (AP-TPE), a fluorescent porous tetraphenylethylene-based organic polymer (**PTOP**) was fabricated with the help of cyanuric chloride. CO_2 sorption measurement at 195 K reveals its permanent porosity nature with a Brunauer-Emmett-Teller surface area of 227 m^2 g^{-1}. Furthermore, rich secondary amines and pyrimidine nitrogen atoms surrounding the 1,3,5-triazine moieties of **PTOP** provide abundant chelating sites for metal ions, which in combination with the porous structure and TPE AIEgen synergistically contribute to the fast-response fluorescence sensing of Fe(III) and nitrobenzene.

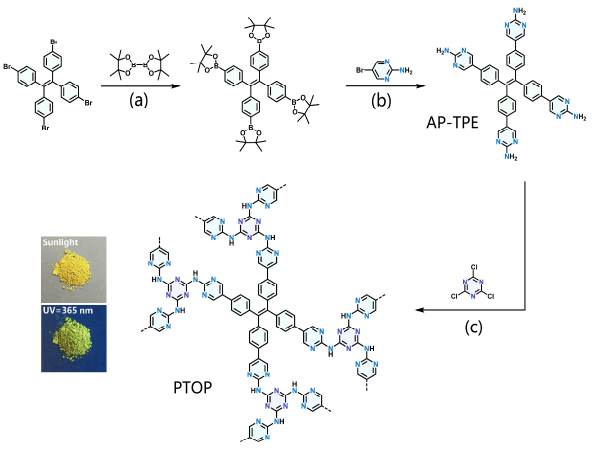

Scheme 1 Synthesis and schematic structure of **PTOP**. (a) KOAc, $Pd(dppf)Cl_2 \cdot CH_2Cl_2$, DME, 100°C, N_2, 12 h; (b) K_2CO_3, $Pd(dppf)Cl_2 \cdot CH_2Cl_2$, 1,4-dioxane, H_2O, 105°C, N_2, 12 h; (c) K_2CO_3, 1,4-dioxane, 90°C,

12 h. (Inset: images under sunlight and 365 nm UV-radiation of **PTOP**, respectively)

2. Experimental Section

2.1 General Directions

All chemicals were employed as received without further purification. 1,1,2,2-tetrakis(4-(4,4,5,5-tetramethyl-1,3,2-dioxaborolan-2-yl)phenyl)ethene (TMDB-TPE), AP-TPE, and **PTOP** were prepared by consulting to the reported methods.[37–39]

2.2 Synthesis of PTOP

Synthesis of TMDB-TPE. A mixture of tetrakis(4-bromophenyl)ethene (0.65 g, 1.0 mmol), bis(pinacolato)diboron (1.50 g, 6.0 mmol), 1,1'-bis(diphenylphosphino)ferrocene-palladium(II)dichloride dichloromethane complex ($Pd(dppf)Cl_2 \cdot CH_2Cl_2$) (0.041 g, 0.05 mmol), and potassium acetate (KOAc) (1.60 g, 16.0 mmol) in 30 mL degassed 1,2-dimethoxyethane (DME) was heated to 100°C for 12 h under N_2. After cooling down, the solvent was removed in vacuum, and the residue was subjected to chromatography on a silica gel column using chloroform as eluent. Repeated column chromatography and the following recrystallization from chloroform and methanol afforded the target white compound TMDB-TPE (0.63 g, yield 75.0%). ^{1}H NMR (400 MHz, $CDCl_3$-d): 7.50 (d, 8H, J = 8.00 Hz), 6.99 (d, 8H, J = 8.00 Hz), 1.32 (s, 48H). MALDI-TOF MS: an isotopic cluster peaking at m/z 836.4, Calcd. for $C_{50}H_{64}B_4O_8$, $[M]^+$ 836.5. Anal. Calcd. for $C_{50}H_{64}B_4O_8 \cdot 0.4CHCl_3$: C, 68.47; H, 7.34. Found: C, 68.43; H, 7.18.

Synthesis of AP-TPE. A mixture of TMDB-TPE (0.40 g, 0.5 mmol), 5-bromopyrimidin-2-amine (0.44 g, 2.5 mmol), $Pd(dppf)Cl_2 \cdot CH_2Cl_2$ (0.012 g, 0.015 mmol), and potassium carbonate (K_2CO_3) (0.69 g, 5.0 mmol) in 1,4-dioxane (20 mL)

and water (5 mL) was stirred at 105°C for 12 h under N_2. The resultant mixture was then cooled to room temperature, filtrated and washed sequentially with water, saturated ammonium chloride aqueous solution, chloroform, and methanol. The pure product AP-TPE was obtained as faint yellow powder (0.25 g, yield 71.7%). ^{1}H NMR (400 MHz, DMSO-d_6): 8.55 (s, 8H), 7.47 (d, 8H, J = 8.00 Hz), 7.08 (d, 8H, J = 8.00 Hz), 6.75 (s, 8H). ^{13}C NMR (400 MHz, DMSO-d_6): 162.79, 155.70, 141.89, 139.70, 133.27, 131.51, 124.40, 121.22. MALDI-TOF MS: an isotopic cluster peaking at m/z 702.9, Calcd. for $C_{42}H_{32}N_{12}$, $[M]^+$ 703.2. Anal. Calcd. for $C_{42}H_{32}N_{12}\cdot 0.5CHCl_3\cdot CH_3OH$: C, 65.59; H, 4.62; N, 21.10. Found: C, 65.55; H, 4.59; N, 21.32.

Synthesis of ***PTOP***. Under nitrogen gas, to a mixture of AP-TPE (0.20 g, 0.28 mmol) and K_2CO_3 (0.12 g, 0.84 mmol) in anhydrous 1,4-dioxane (15 mL), an 1,4-dioxane (2 mL) solution of CC (0.068 g, 0.37 mmol) was slowly added at room temperature. The mixture was stirred at 90°C for 12 h. The resulting precipitate was collected by filtration and washed with water, N,N-dimethylformamide (DMF), and methanol to remove the unreacted starting precursors. The product was dried in vacuum at 50°C, affording the bright yellow powder with a yield of 76.1 % (0.17 g). Anal. found: C, 62.42; H, 4.34; N, 21.88.

2.3 Instrumental characterization

MALDI-TOF mass spectrum was taken on a Bruker BIFLEX III ultra-high resolution Fourier transform ion cyclotron resonance (FT-ICR) mass spectrometer with a-cyano-4-hydroxycinnamic acid as the matrix. NMR spectra were recorded on a Bruker DPX 400 spectrometer in indicated solvent and referenced internally using the respective typical residual solvent resonances relative to $SiMe_4$. Solid-state NMR spectra were collected

on a 400 MHz Bruker Avance III spectrometer. Fourier transform infrared spectra (FT-IR) were recorded as KBr pellets using a Bruker Tensor 37 spectrometer with 2 cm^{-1} resolution. Elemental analysis data were carried out on Elementar Vavio El III elemental analyzer. Thermal gravimetric analysis (TGA) datum was collected on a PerkinElmer TG-7 analyzer with a heating rate of 5°C min^{-1} in the range of 25~800°C under N_2 atmosphere. Scanning electron microscope (SEM) image was obtained using a JEOL JEM-6510A scanning electron microscopy. Transmission electron microscopy (TEM) photo was provided by HT7700 electron microscope. Steady-state fluorescence spectroscopic studies were performed on F4500 (Hitachi) analyzer. X-ray photoelectron spectra (XPS) data were collected from PHI 5300 ESCA System (PerkineElmer, USA). The sorption isotherms were obtained using a Micromeritics ASAP 2020 surface area analyzer.

2.4 Measurement for gas adsorption

Before the gas sorption measurements, the powder sample of **PTOP** was degassed at 100°C for 12 hours to drastically eliminate the volatile solvents blocked in pores. The porous nature was examined with N_2 and CO_2 as adsorbate. The sorption isotherms were collected at 77, 195, 273, and 298 K, maintaining in a bath of liquid nitrogen, dry ice/acetone slurry, an ice/water mixture, and water in an air-conditioned 23°C laboratory, respectively.

2.5 Sensing experiments for metal ions and aromatic derivatives

Prior to sensing experiments, **PTOP** (0.25 mg) was sonicated in methanol (1.0 mL) for 20 minutes to ensure the well dispersion. For the metal ions sensing experiments, the fluorescence detection was performed by adding the methanol solution of different metal ions (Na^+, Mg^{2+}, Al^{3+}, K^+, Fe^{2+}, Fe^{3+}, Co^{2+}, Ni^{2+}, Cu^{2+}, Zn^{2+}, Ag^+, Cd^{2+}, Ba^{2+}, Hg^{2+}, and Pb^{2+}, respectively) into a quartz cuvette containing a suspension of **PTOP**.

With regard to the aromatic derivatives detection experiments, aromatic solvent (toluene, paraxylene, mesitylene, benzaldehyde, chlorobenzene, benzonitrile, benzoic acid, phenol, and nitrobenzene, respectively) was added into a quartz cuvette containing a methanol solution of **PTOP** in well dispersed form.

3. Results and Discussion

3.1 Synthesis and characterization

The purity of AP-TPE has been checked by MS spectra and NMR spectra, Fig. S1. **PTOP** was synthesized through the reaction between AP-TPE and CC with the assistance of K_2CO_3, Scheme 1. As mentioned above, the existence of rich pyrimidine nitrogen atoms and amino groups surrounding the 1,3,5-triazine segments inside the pores of **PTOP** creates abundant potential chelating sites for metal ions.

Fig. 1a shows the solid state ^{13}C CP/MAS NMR spectrum of **PTOP** with resonance signals appearing at 164.4, 158.2, 144.5, 134.7, 127.2 and 125.7 ppm. With the aid of ^{13}C NMR spectrum of AP-TPE in DMSO-d_6 (Fig. S1c), the signal of **PTOP** at approximately 144.5 ppm is unambiguously assigned to the ethylene carbon atoms, the peaks at 144.5, 134.7, and 127.2 ppm attributed to benzene carbon atoms, and those at 164.4, 158.2, and 125.7 ppm due to the pyrimidine carbon atoms. In addition, triazine carbon atoms also contribute to the overlapped signal at 164.4 ppm.

Fourier transform infrared spectroscopy (FT-IR) was also used to illustrate the successful formation of **PTOP**. The FT-IR spectra of AP-TPE, CC, and **PTOP** are compared in Fig. 1b. As can be seen, the absorption at 3399 cm^{-1} due to the -NH_2 stretching vibration for AP-TPE got significantly decreased relative after the formation of **PTOP**. In addition, new bands appear at 1715 and 1426 cm^{-1} after the integration of triazine moieties with AP-TPE, confirming the formation of **PTOP**.

As exhibited from thermal gravimetric analysis (TGA) curve of **PTOP** in Fig. S2, this material experiences a gradual weight loss of 8.0% from room temperature to 270°C, due to the release of volatile solvent molecules embedded inside the pores of **PTOP**. After that, the organic component keeps stable until 440°C and then rapidly decomposes along with further increasing the temperature.

The morphology of **PTOP** was studied first by scanning electron microscope (SEM), Fig. 1c, indicating the formation of a peony-like cluster assembled from nanosheets, and transmission electron microscope (TEM) further revealed the layer-like **PTOP**, Fig. 1d.

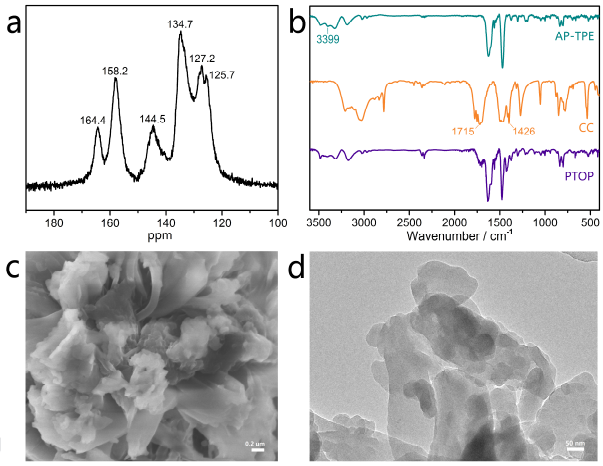

Fig. 1 Various characterization of **PTOP** including solid state ^{13}C CP/MAS NMR spectrum (a), FT-IR spectra (b), SEM image (c), and TEM diagram (d).

3.2 Gas adsorption studies

Towards inspecting the porous nature of **PTOP**, gas sorption experiments using N_2 and CO_2 as adsorbate, respectively, were carried out. The result indicates that **PTOP** does not adsorb any nitrogen at 77 K, possibly due to the existence of narrow pores, which hinder the N_2 gas diffusion into the pores. This, however, is not true for CO_2 because of the smaller kinetics diameter of 3.3 Å of CO_2 than that of N_2 molecule, 3.64 Å.[40] As shown in Fig. 2, the CO_2 sorption isotherm of **PTOP** at 195 K shows a typical type I character, disclosing the

microporous nature of **PTOP**. The experimental Brunauer-Emmett-Teller (BET) surface area amounts to 227 m^2 g^{-1}. In addition, the CO_2 adsorption isotherms of **PTOP** at 273 and 298 K were also determined, showing the uptakes at 760 mmHg of 22 and 15 cm^3 g^{-1}, respectively, confirming the porous nature of **PTOP**. According to the virial equation,[41,42] the isosteric heat of 28.8 kJ mol^{-1} was calculated by fitting the adsorption isotherms measured at 273 and 298 K. Obviously, the existence of the permanent porosity for **PTOP** would be favorable to the diffusion of analyte in sensing.

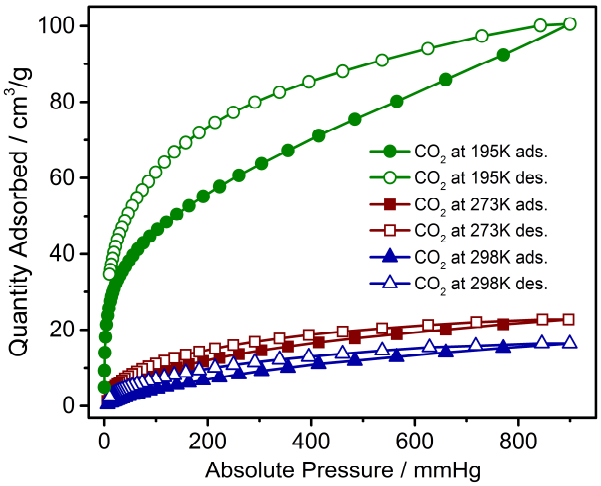

Fig. 2 CO_2 adsorption and desorption of **PTOP** at 195, 273 and 298 K, respectively.

3.3 Detection of metal ions

TPE is a typical AIE chromophore. After integration of four 2-aminopyrimidin groups with a TPE unit, the new obtained AP-TPE in DMF exhibits a very weak emission, Fig. S3. After increasing H_2O content in H_2O/DMF solution to 30%, there suddenly appears a strong emission at 517 nm, Fig. S3b. When the H_2O content was further gradually increased to 70%, the emission maximum of AP-TPE undergoes the blue shifts from 526 to 506 nm and the increased fluorescence intensity. The blue-shift at lower water fraction is originated from the formation of a higher ordered microstructure following the increase of water fraction.[43,44] By increasing the

content of H_2O to 90%, the fluorescence intensity of AP-TPE was reduced because of aggregation effect and the emission maximum was gradually red-shifted back to 525 nm. These results clearly disclose the presence of aggregation-induced emission, confirming the newly fabricated AP-TPE being AIE-active. The combination of AP-TPE into porous organic polymers must result in an AIE-confined fluorescence species.

As can be found in Fig. S4, the emission peak position of **PTOP** (0.25 mg/mL dispersion solution) slightly depends the solvent species. In detail, the maximum emission of this material keeps constant at ca. 507 nm in DMF, N,N-dimethylacetamide (DMA), methanol (MeOH), ethanol, acetone, tetrahydrofuran (THF), ethyl acetate, chloroform, and toluene, but displays a slight blue shift in the narrow range of 0~5 nm for water, acetonitrile, or n-hexane. However, the fluorescence intensity of **PTOP** shows a solvent-dependent character associated with the solvent polarity effect.[45] Since **PTOP** in methanol exhibits the strongest emission intensity among all solvents, the subsequent sensing experiments were carried out in methanol as detailed below.

For the purpose of studying the sensing properties of **PTOP** towards metal species, its fluorescence properties were investigated by adding the methanol solution of a series of metal ions including Na^+, Mg^{2+}, Al^{3+}, K^+, Fe^{2+}, Fe^{3+}, Co^{2+}, Ni^{2+}, Cu^{2+}, Zn^{2+}, Ag^+, Cd^{2+}, Ba^{2+}, Hg^{2+}, and Pb^{2+} (10 mM) into the methanol suspension of **PTOP**. According to the experimental results, addition of Na^+ and Mg^{2+} solution induces a slight increase in the fluorescence intensity, while addition of the other metal ions leads to the varying fluorescence quenching phenomena depending on the metal species, Fig. 3a and S5a. It is well known that the sensing performance of the fluorescent sensor is closely dependent on both the selective binding of receptor to

detected target and the accordingly signal change of the fluorescent unit.[46,47] As a consequence, the fluorescent sensor will exhibit selective sensing function towards different targets. This is also true for target metal ions. However, the essential reason behind the different quenching of fluorescence sensor for different metal ions such K^+ *vs*. Pb^{2+}/Hg^{2+} is still not clear at the present stage. Interestingly, the fluorescence of **PTOP** is completely quenched after addition of Fe^{3+}. In addition to the selective binding between the sensor and Fe^{3+} rather than other metal ions such as Pb^{2+} and Co^{2+}, the present great quenching of Fe^{3+} on the fluorescence sensor might be also due to the synergistic effect of *d* orbit and paramagnetism, which is consistent with the reported literature.[48-50] In addition, time-dependent sensing experimental towards Fe^{3+} ion indicates the immediate emission quenching flowing the Fe^{3+} addition, Fig. 3b.

Furthermore, interference experiments were carried out for **PTOP** by simultaneously introducing Fe^{3+} ions (10 mM, 1.0 mL) and other metal ions (10 mM, 1.0 mL) into the suspension (0.5 mL) of **PTOP** at room temperature. Even in the presence of various interference cations, the quenching effect of the Fe^{3+} ions on the emission of **PTOP** was still significant, Fig. S5b, further confirming the high-selective sensing capability of this porous organic polymer towards Fe^{3+} ions.

Given the fact that excess amount of Fe^{3+} ion is harmful for human organisms, developing selective and sensitive sensors for Fe^{3+} therefore is of significant importance. To qualitatively investigate the quenching sensitivity of **PTOP** towards Fe^{3+} analyte, the fluorescence spectra of **PTOP** were determined in different concentrations of Fe^{3+} ion, Fig. 3c. According to the Stern-Volmer equation $I_0/I=1+K_{sv}[M]$[49,51] (I_0: the initial fluorescence intensity in the absence of Fe^{3+}; I: the fluorescence intensity in the presence of Fe^{3+}; K_{sv}: the quenching constant; [M]: the molar concentration of Fe^{3+} analyte), quenching constant K_{sv} of 5.6 mM^{-1} for **PTOP**

towards Fe^{3+} was deduced on the basis of experimental results, Fig. 3d. This in turn gives the limit of detection (LOD) concentration of 4.5 μM for **PTOP** towards fluorescence sensing Fe^{3+} according to the equation $3\sigma/K_{sv}$ (σ: standard deviation), which is lower than that for most previously reported fluorescent sensing materials towards Fe^{3+} ion.[52–54] Towards the practical use, the sensitivity of **PTOP** to detect Fe^{3+} ion in aqueous solution was also tested, and the detection limit of **PTOP** was calculated to be 7.0 μM by the same method, as shown in Fig. S6. In the present case, the LOD of **PTOP** for Fe^{3+} in aqueous solution is also obviously lower than the drinking water hygiene standard of 0.3 mg/L (5.4 mM) proposed by "drinking water sanitary standard" (GB5749-2006) of People's Republic of China[55] as well as the international standard water quality index and limit value (0.3 mg/L),[56] indicating the future practical application potential of the newly developed **PTOP**.

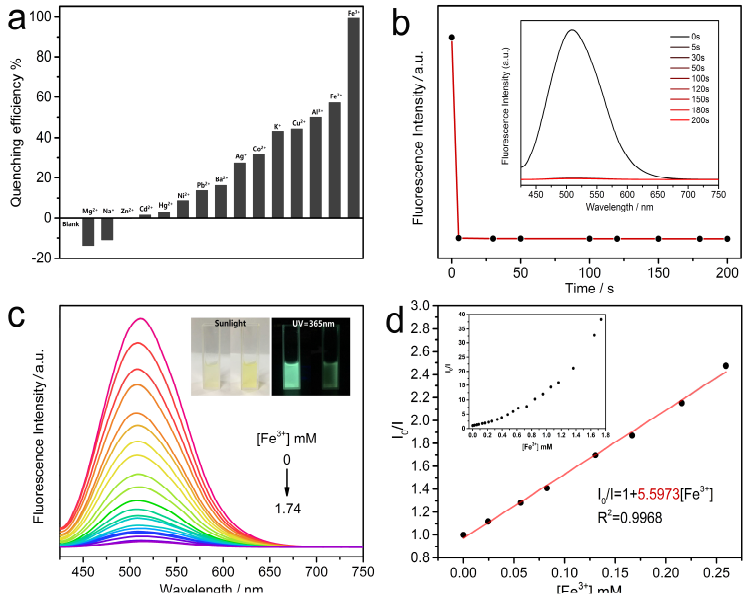

Fig. 3 (a) Quenching efficiency of **PTOP** immersed in MeOH solutions of different metal ions. (b) The time-dependent emission intensity (at 507 nm) of **PTOP** immersed in a MeOH solution of Fe^{3+} ion (inset: the time-dependent emission spectra under the excitation wavelength of 410 nm). (c) Emission spectra by the gradual addition of a Fe^{3+} methanol solution (inset: images under sunlight and 365 nm UV-radiation of **PTOP** (left) and **PTOP**@Fe^{3+} (right), respectively). (d) K_{sv} curve of **PTOP** immersed in MeOH solutions

of Fe^{3+} ion with different concentrations (insert: the changed I_0/I curve with the increased concentration of Fe^{3+} ion).

Towards understanding the fluorescence quenching mechanism of **PTOP** by Fe^{3+}, X-ray photoelectron spectroscopic (XPS) studies were conducted on the Fe^{3+}-tested material (denoted as **PTOP**@Fe^{3+}). As can be seen from Fig. 4a, besides C and N elements, XPS spectrum of **PTOP**@Fe^{3+} also displays the Fe^{3+} element signal at the binding energy of 711.0 eV,[57] indicating the inclusion of Fe^{3+} within the pores of **PTOP**. Nevertheless, the peak due to the combination of sp^2 (-C=N) and sp^3 (-NH) nitrogen atoms at the binding energy of 398.4 eV in the high-resolution N 1s XPS spectrum of **PTOP** takes a slight up-shift to 398.6 eV for **PTOP**@Fe^{3+}, Fig. 4b, suggesting the existence of interaction between Fe^{3+} cations and imine group basic sites in **PTOP**@Fe^{3+}.

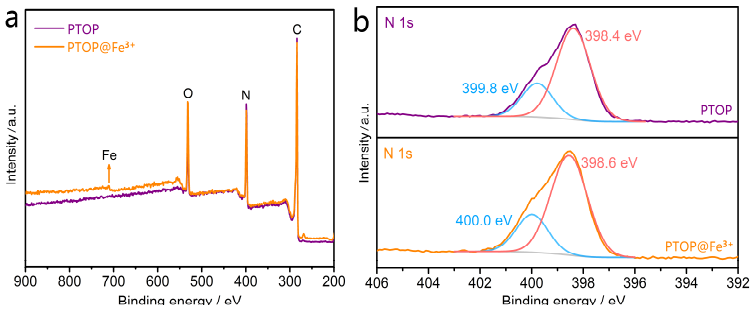

Fig.4 XPS spectra (a) and N 1s XPS spectra (b) for **PTOP** (purple) and **PTOP**@Fe^{3+} (orange).

3.4 Detection of aromatic derivatives

As mentioned above, the wide range of industrial and biochemical application of various nitroaromatic compounds not only contaminates the environment but also seriously threats human health.[58] It is therefore important to develop the effective fluorescent sensors for such kind of organic compounds. As a consequence, the fluorescence properties of **PTOP** were also investigated in the presence of a series of aromatic derivatives. As shown in Fig. 5a and b, the emission of **PTOP** was not

influenced by adding the aromatic analytes including toluene, paraxylene, mesitylene, benzaldehyde, chlorobenzene, benzonitrile, benzoic acid, and phenol into the methanol of **PTOP**. In contrast, addition of nitrobenzene (NB), the exemplary and harmful explosive, leads to a sharp fluorescence quenching of **PTOP** due probably to the electron transfer from the polymer to analyte,[59,60] indicating the high selectivity of **PTOP** toward NB over other aromatic compounds. The quenching process was also monitored by the time-dependent emission intensity at the maximum peak, Fig. S7, revealing the occurrence of immediate fluorescence quenching. Studies over the change of emission intensity as a response of the added NB concentration revealed that addition of NB even with the concentration as low as 14.7 nM induces a serious fluorescence quenching of **PTOP**, Fig. 5c. When increasing the concentration of NB introduced to 0.6 μM, the fluorescence signal got almost completely disappeared. Aiming for identifying the quenching constant of **PTOP** towards NB, the Stern-Volmer equation was employed again. As shown in Fig. 5d, from the linear fitting, the quenching constant K_{sv} of 16.3 μM^{-1} between **PTOP** and NB was deduced, with the LOD of **PTOP** being determined to be 1.6 nM according to $3\sigma/K_{sv}$. This value again is much lower than the excellent fluorescent materials for nitrobenzene detection reported previously,[61–65] indicating the good selectivity and high sensitivity of **PTOP** to NB.

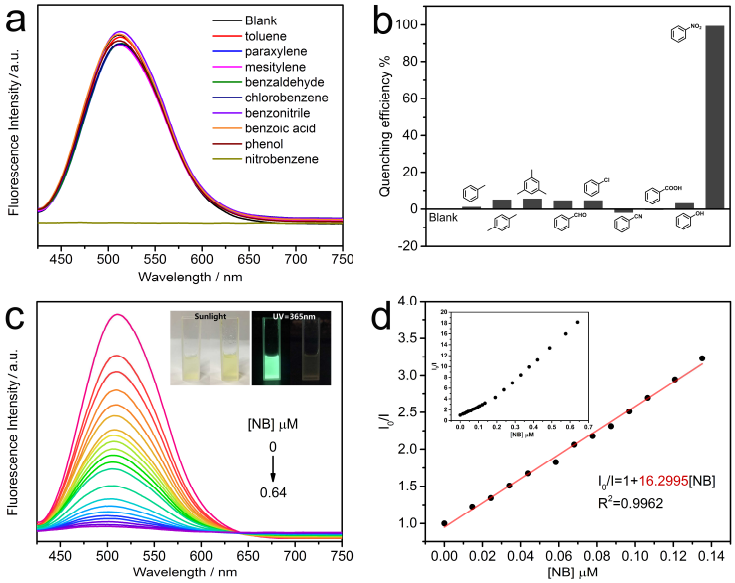

Fig. 5 Emission spectra (a) and quenching efficiency (b) of **PTOP** immersed into the MeOH solutions of different aromatic compounds. (c) Emission spectra by the gradual addition of a NB methanol solution (inset: images under sunlight and 365 nm UV-radiation of **PTOP** (left) and **PTOP**@NB (right), respectively). (d) K_{sv} curve of **PTOP** immersed in MeOH solutions of NB with different concentrations (insert: the changed I_0/I curve with the increased concentration of NB).

4. Conclusion

Briefly summarizing above, a new TPE-based porous organic polymer has been fabricated and characterized. The permanent porosity, TPE AIEgen, and rich chelating sites synergistically contribute to the immediate fluorescence sensing of Fe(III) and nitrobenzene with high selectivity and sensitivity. In particular, the limit of detection concentration of **PTOP** for fluorescent sensing Fe^{3+} is much lower than the international standard water quality index, suggesting its good future practical applications.

Acknowledgements

Financial support from the Natural Science Foundation of China (Nos. 21631003 and

21805005), the Fundamental Research Funds for the Central Universities (No. FRF-BD-17-016A and FRF-BR-18-009B), and University of Science and Technology Beijing is gratefully acknowledged.

References

[1] Seo M, Kim S, Oh J, Kim SJ, Hillmyer MA. Hierarchically porous polymers from hyper-cross-linked block polymer precursors. J Am Chem Soc 2015;137:600–3.

[2] McKeown NB, Gahnem B, Msayib KJ, Budd PM, Tattershall CE, Mahmood K, et al. Towards polymer-based hydrogen storage materials: engineering ultramicroporous cavities within polymers of intrinsic microporosity. Angew Chem Int Ed 2006;21:1804–7.

[3] Han S, Mendoza-Cortés JL, Goddard III WA. Recent advances on simulation and theory of hydrogen storage in metal-organic frameworks and covalent organic frameworks. Chem Soc Rev 2009;38:1460–76.

[4] Kuhn P, Antonietti M, Thomas A. Porous, covalent triazine-based frameworks prepared by ionothermal synthesis. Angew Chem Int Ed 2008;47:3450–3.

[5] Xu Y, Jin S, Xu H, Nagai A, Jiang D. Conjugated microporous polymers: design, synthesis and application. Chem Soc Rev 2013;42:8012–31.

[6] Cooper A I. Conjugated microporous polymers. Adv Mater 2009;21:1291–5.

[7] Li B, Zhang Y, Krishna R, Yao K, Han Y, Wu Z, et al. Introduction of π-complexation into porous aromatic framework for highly selective adsorption of ethylene over ethane. J Am Chem Soc 2014;136:8654–60.

[8] Ben T, Ren H, Ma S, Cao D, Lan J, Jing X, et al. Targeted synthesis of a porous aromatic framework with high stability and exceptionally high surface area. Angew Chem Int Ed 2009;48:9457–60.

[9] Ben T, Pei C, Zhang D, Xu J, Deng F, Jing X, et al. Gas storage in porous aromatic frameworks (PAFs). Energy Environ Sci 2011;4:3991–9.

[10] Lu W, Yuan D, Zhao D, Schilling C, Plietzsch O, Muller T, et al. Porous polymer networks: synthesis, porosity, and applications in gas storage/separation. Chem Mater 2010;22:5964–72.

[11] Rodenas T, Luz I, Prieto G, Seoane B, Miro H, Corma A, et al. Metal-organic framework nanosheets in polymer composite materials for gas separation. Nat Mater 2015;14:48–55.

[12] Farha OK, Spokoyny AM, Hauser BG, Bae Y, Brown SE, Snurr RQ, et al. Synthesis, properties, and gas separation studies of a robust diimide-based microporous organic polymer. Chem Mater 2009;21:3033–5.

[13] Alsbaiee A, Smith BJ, Xiao L, Ling Y, Helbling DE, Dichtel WR. Rapid removal of organic micropollutants from water by a porous β-cyclodextrin polymer. Nature 2016;529:190–4.

[14] Chen L, Furukawa K, Gao J, Nagai A, Nakamura T, Dong Y, et al. Photoelectric covalent organic frameworks: converting open lattices into ordered donor-acceptor heterojunctions. J Am Chem Soc 2014;136:9806–9.

[15] Horike S, Umeyama D, Kitagawa S. Ion conductivity and transport by porous coordination polymers and metal-organic frameworks. Acc Chem Res 2013;46:2376–84.

[16] Kreno LE, Leong K, Farha OK, Allendorf M, Van Duyne RP, Hupp JT, Metal-organic framework materials as chemical sensors. Chem Rev 2012;112:1105–25.

[17] Kaur P, Hupp JT, Nguyen ST. Porous organic polymers in catalysis: opportunities and challenges. ACS Catal 2011;1:819–35.

[18] Wu C, Hu A, Zhang L, Lin W. A homochiral porous metal-organic framework for highly enantioselective heterogeneous asymmetric catalysis. J Am Chem Soc

2005;127:8940–1.

[19] Luo J, Xie Z, Lam JWY, Cheng L, Chen H, Qiu C, et al. Aggregation-induced emission of 1-methyl-1,2,3,4,5-pentaphenylsilole. Chem Commun 2001;0:1740–1.

[20] Hong Y, Lam JWY, Tang BZ. Aggregation-induced emission. Chem Soc Rev 2011;40:5361–88.

[21] Mei J, Leung NLC, Kwok RTK, Lam JWY, Tang BZ. Aggregation-induced emission: together we shine, united we soar! Chem Rev 2015;115:11718–940.

[22] Wang H, Li B, Wu H, Hu TL, Yao Z, Zhou W, Xiang S, Chen B, A flexible microporous hydrogen-bonded organic framework for gas sorption and separation. J Am Chem Soc 2015;137:9963–70.

[23] Wang H, Bao Z, Wu H, Lin RB, Zhou W, Hu TL, Li B, Zhao JCG, Chen B, Two solvent-induced porous hydrogen-bonded organic frameworks: solvent effects on structures and functionalities. Chem Commun 2017;53:11150–3.

[24] Dalapati S, Jin E, Addicoat M, Heine T, Jiang D. Highly emissive covalent organic frameworks. J Am Chem Soc 2016;138:5797–800.

[25] Shustova NB, McCarthy BD, Dincă M. Turn-on fluorescence in tetraphenylethylene-based metal-organic frameworks: an alternative to aggregation-induced emission. J Am Chem Soc 2011;133:20126–9.

[26] Guo Y, Feng X, Han T, Wang S, Lin Z, Dong Y, et al. Tuning the luminescence of metal-organic frameworks for detection of energetic heterocyclic compounds. J Am Chem Soc 2014;136:15485–8.

[27] Liu Y, Deng C, Tang L, Qin A, Hu R, Sun J, et al. Specific detection of D-glucose by a tetraphenylethene-based fluorescent sensor. J Am Chem Soc 2011;133:660–3.

[28] Tong H, Hong Y, Dong Y, Häußler M, Lam JWY, Li Z, et al. Fluorescent “light-up” bioprobes based on tetraphenylethylene derivatives with aggregation-induced emission

characteristics. Chem Commun 2006;35:3705–7.

[29] Wei Y, Chen W, Zhao X, Ding S, Han S, Chen L. Solid-state emissive cyanostilbene based conjugated microporous polymers via cost-effective Knoevenagel polycondensation. Polym Chem 2016;7:3983–8.

[30] Ma T, Zhao X, Matsuo Y, Song J, Zhao R, Faheem M, et al. Fluorescein-based fluorescent porous aromatic framework for Fe^{3+} detection with high sensitivity. J Mater Chem C 2019;7:2327–32.

[31] Yu C, Sun X, Zou L, Li G, Zhang L, Liu Y. A pillar-layered Zn-LMOF with uncoordinated carboxylic acid sites: high performance for luminescence sensing Fe^{3+} and TNP. Inorg Chem 2019;58:4026–32.

[32] Pu Y, Yu Z, Wang F, Fu Y. Selective fluorescence sensing of *p*-nitroaniline and Fe^{3+} ions by luminescent Eu-based metal-organic framework. Sensor Rev 2019;39:149–61.

[33] Zhang X, Zhuang X, Zhang N, Ge C, Luo X, Li J, et al. A luminescent sensor based on a Zn (ii) coordination polymer for selective and sensitive detection of NACs and Fe^{3+} ions. Cryst Eng Comm 2019;21:1948–55.

[34] Guo L, Zeng X, Cao D. Porous covalent organic polymers as luminescent probes for highly selective sensing of Fe^{3+} and chloroform: functional group effects. Sensor Actuat B: Chem 2016;226:273–8.

[35] Dong J, Li X, Zhang K, Yuan Y, Wang Y, Zhai L, et al. Confinement of aggregation-induced emission molecular rotors in ultrathin two-dimensional porous organic nanosheets for enhanced molecular recognition. J Am Chem Soc 2018;140:4035–46.

[36] Wei F, Cai X, Nie J, Wang F, Lu C, Yang G, et al. A 1,2,3-triazolyl based conjugated microporous polymer for sensitive detection of *p*-nitroaniline and Au nanoparticle immobilization. Polym Chem 2018;9:3832–9.

[37] Liu Y, Mu C, Jiang K, Zhao J, Li Y, Zhang L, et al. A tetraphenylethylene core-based 3D structure small molecular acceptor enabling efficient non-fullerene organic solar cells. Adv Mater 2015;27:1015–20.

[38] Lai Y, Chang C. Photostable BODIPY-based molecule with simultaneous type I and type II photosensitization for selective photodynamic cancer therapy. J Mater Chem B 2014;2:1576–83.

[39] Ma H, Kan J, Chen G, Chen C, Dong Y. Pd NPs-loaded homochiral covalent organic framework for heterogeneous asymmetric catalysis. Chem Mater 2017;29:6518–24.

[40] Mondal SS, Bhunia A, Kelling A, Schilde U, Janiak C, Holdt H. Giant Zn_{14} molecular building block in hydrogen-bonded network with permanent porosity for gas uptake. J Am Chem Soc 2014;136:44–7.

[41] Wen HM, Liao C, Li L, Alsalme A, Alothman Z, Krishna R, et al. A metal-organic framework with suitable pore size and dual functionalities for highly efficient post-combustion CO_2 capture. J Mater Chem A 2019;7:3128–34.

[42] Wen HM, Li L, Lin RB, Li B, Hu B, Zhou W, Hu J, Chen B. Fine-tuning of nano-traps in a stable metal-organic framework for highly efficient removal of propyne from propylene. J Mater Chem A 2018;6:6931–7.

[43] Huang Y, Mei J, Ma X. A novel simple red emitter characterized with AIE plus intramolecular charge transfer effects and its application for thiol-containing amino acids detection. Dyes Pigments 2019;165:499–507.

[44] Bai W, Wang Z, Tong J, Mei J, Qin A, Sun JZ, Tang BZ. A self-assembly induced emission system constructed by the host–guest interaction of AIE-active building blocks. Chem Commun 2015;51:1089–91.

[45] Yan X, Cook TR, Wang P, Huang F, Stang PJ. Highly emissive platinum (II) metallacages. Nat Chem 2015;7:342–8.

[46] Ballesteros E, Moreno D, Gómez T, Rodríguez T, Rojo J, García-Valverde M, et al. A new selective chromogenic and turn-on fluorogenic probe for copper(II) in water-acetonitrile 1:1 solution. Org Lett 2009;11:1269–72.

[47] Zhang X, Hayes D, Smith SJ, Friedle S, Lippard SJ. New strategy for quantifying biological zinc by a modified zinpyr fluorescence sensor. J Am Chem Soc 2008;130:15788–9.

[48] Ding W, Xu J, Wen Y, Zhang J, Liu H, Zhang Z. Highly selective “turn-on” fluorescent sensing of fluoride ion based on a conjugated polymer thin film-Fe^{3+} complex. Anal Chim Acta 2017;967:78–84.

[49] Liu J, Zhong Y, Lu P, Hong Y, Lam JWY, Faisal M, et al. A superamplification effect in the detection of explosives by a fluorescent hyperbranched poly (silylenephenylene) with aggregation-enhanced emission characteristics. Polym Chem 2010;1:426–9.

[50] Zhang Z, Li F, He C, Ma H, Feng Y, Zhang Y, et al. Novel Fe^{3+} fluorescence probe based on the charge-transfer (CT) molecules. Sensor Actuat B: Chem 2018;255:1878–83.

[51] Wang H, Wang D, Wang Q, Li X, Schalley CA. Nickel (II) and iron (III) selective off-on-type fluorescence probes based on perylene tetracarboxylic diimide. Org Biomol Chem 2010;8:1017–26.

[52] Namgung H, Kim J, Gwon Y, Lee T. Synthesis of poly (p-phenylene) containing a rhodamine 6G derivative for the detection of Fe (III) in organic and aqueous media. RSC Adv 2017;7:39852–8.

[53] Huang Y, Chen H, Wang Y, Ren Y, Li Z, Li L, et al. A channel-structured Eu-based metal-organic framework with a zwitterionic ligand for selectively sensing Fe^{3+} ions. RSC Adv 2018;8:21444–50.

[54] Chen X, Zhao Q, Zou W, Qu Q, Wang F. A colorimetric Fe^{3+} sensor based on an anionic poly(3,4-propylenedioxythiophene) derivative. Sensor Actuat B: Chem

2017;244:891–6.

[55] Baidu Baike of China, https://baike.baidu.com/item/GB5749-2006/6553808?fr=aladdin

[56] World Health Organization, Guidelines for drinking-water quality: fourth edition incorporating the first addendum, 2017.

[57] Zhu J, Chen F, Zhang J, Chen H, Anpo M. Fe^{3+}-TiO_2 photocatalysts prepared by combining sol-gel method with hydrothermal treatment and their characterization. J Photoch Photobio A 2006;180:196–204.

[58] Pramanik S, Zheng C, Zhang X, Emge TJ, Li J. New microporous metal-organic framework demonstrating unique selectivity for detection of high explosives and aromatic compounds. J Am Chem Soc 2011;133:4153–5.

[59] Shanmugaraju S, Jadhav H, Karthikb R, Mukherjee PS. Electron rich supramolecular polymers as fluorescent sensors for nitroaromatics. RSC Adv 2013;3:4940–50.

[60] Li J, Liu J, Lam JWY, Tang BZ. Poly(arylene ynonylene) with an aggregation-enhanced emission characteristic: a fluorescent sensor for both hydrazine and explosive detection. RSC Adv 2013;3:8193–6.

[61] Rameshkumar P, Viswanathan P, Ramaraj R. Silicate sol-gel stabilized silver nanoparticles for sensor applications toward mercuric ions, hydrogen peroxide and nitrobenzene. Sensor Actuat B: Chem 2014;202:1070–7.

[62] Rastogi PK, Ganesan V, Krishnamoorthi S. Palladium nanoparticles incorporated polymer-silica nanocomposite based electrochemical sensing platform for nitrobenzene detection. Electrochim Acta 2014;147:442–50.

[63] Liu L, Chen J, Yu C, Lv W, Yu H, Cui X, Liu L. A novel Ag(I)-calix[4]arene coordination polymer for the sensitive detection and efficient photodegradation of

nitrobenzene in aqueous solution. Dalton Trans 2017;46:178–85.

[64] Wu W, Liu P, Liang Y, Cui L, Xi Z, Wang Y. Three luminescent d^{10} metal coordination polymers assembled from a semirigid V-shaped ligand with high selective detecting of Cu^{2+} ion and nitrobenzene. J Solid State Chem 2015;228:124–30.

[65] Shi M, Yang J, Liu Y, Ma J. Four coordination polymers based on 1,4,8,11-tetrazacyclotetradecane-N,N',N'',N'''-tetra-methylene-benzoic acid: syntheses, structures, and selective luminescence sensing of iron (III) ions, dichromate anions, and nitrobenzene. Dyes Pigments 2016;129:109–20.

Highlights

- A fluorescent porous tetraphenylethylene-based organic polymer (**PTOP**) was constructed.
- CO_2 sorption experiment reveals that the BET surface area of **PTOP** is 227 $m^2 g^{-1}$.
- **PTOP** endows a fast-response and sensitive fluorescence sensing Fe(III) and nitrobenzene with a low limit of detection of 4.5 μM and 1.6 nM, respectively.